

## Superlensing plano-convex-microsphere (PCM) lens for direct laser nano-marking and beyond

BING YAN,<sup>1,2</sup> LIYANG YUE,<sup>1</sup> JAMES NORMAN MONKS,<sup>1</sup> XIBIN YANG,<sup>2,4</sup> DAXI XIONG,<sup>2</sup> CHUNLEI JIANG,<sup>3</sup> AND ZENGBO WANG<sup>1,\*</sup> 

<sup>1</sup>School of Computer Science and Electronic Engineering, Bangor University, Dean Street, Bangor, Gwynedd, LL57 1UT, UK

<sup>2</sup>Center of Optics Health, Suzhou Institute of Biomedical Engineering and Technology, Chinese Academy of Sciences, No. 88 Keling Street, Suzhou, Jiangsu 215163, China

<sup>3</sup>College of Electrical and Information Engineering, Northeast Petroleum University, Daqing 163318, China

<sup>4</sup>e-mail: yangxb@sibet.ac.cn

\*Corresponding author: z.wang@bangor.ac.uk

Received 17 October 2019; revised 2 December 2019; accepted 7 December 2019; posted 3 January 2020 (Doc. ID 380574); published 21 February 2020

**A high-performance all-dielectric lens, formed by integrating a conventional plano-convex lens with a high-index microsphere lens (PCM), was developed for far-field super-resolution applications. The PCM lens features a theoretical resolution of  $\sim \lambda/2.5$  in air with a WD  $\sim 2 \mu\text{m}$  away from the lens. When combined with a femtosecond laser, the actual patterning resolution can reach  $\sim \lambda/3.5$ . The unusual focusing properties were theoretically and experimentally verified, and direct laser nano-writing of arbitrary patterns and nanostructures on various substrates was demonstrated. This Letter can be naturally extended to other super-resolution applications, including imaging, sensing, and trapping, with the potential of developing next-generation low-cost direct laser nano-marking machine and super-resolution imaging nanoscope.** © 2020 Optical Society of America

<https://doi.org/10.1364/OL.380574>

The laser has been recognized as one of the most extensively used tools for micro/nano-patterning. Complicated structures can be precisely generated through a non-contact and maskless laser direct-writing. However, the key challenge of laser processing to produce extremely small features is the optical diffraction limit [1]. To overcome such difficulty, various laser-based techniques have emerged for sub-diffraction nano-texturing, such as near-field scanning optical microscope patterning [2,3], laser combination with scanning probe microscopy tip patterning [2,4], plasmonic lithography [5], laser thermal lithography [6], interference lithography [7,8], as well as multiphoton absorption lithography [9,10], etc. However, these techniques were limited in laboratory stage due to their low throughput and sophisticated control system.

Recently, using dielectric microsphere as a near-field lens for super-resolution nano-imaging and fabrication has attracted great interest. The optical phenomenon known as photonic nanojet can contribute to laser beam focusing to break the diffraction limit [11–13]. Researchers have

achieved sub-diffraction features ( $\sim \lambda/3$ ) through a laser-induced particle-lens technique [14,15]. In order to increase the throughput, a contacting particle-lens array (CPLA) technique was also introduced. This method employs a monolayer close-packed particle-lens array to split a laser beam into multiple enhanced focal spots to generate parallel nano-features over a large area [16–18]. On this basis, Guo *et al.* has improved and innovated a kind of arbitrary-shaped patterning technique by an adjustable angular incident laser beam [19].

Although the CPLA has been proven to be a simple and highly productive strategy for nano-fabrication on various materials, there are some inevitable limitations. The target substrate for preparing a preliminary self-assembly monolayer has to be hydrophilic which implies the inadaptability of a hydrophobic surface [20]. Furthermore, the ejection of microspheres generally happens after a single laser shot, which may be due to thermal expansion of substrate caused by laser absorption [21]. Therefore, the substrate dependency and non-reusable factor make it impossible for industry use. Several techniques were proposed to circumvent these issues, usually by transferring the CPLA to transparent host media [22–24]. Although multi-pulse processing is feasible by this method, the series of techniques still lack reliability and cannot produce user-defined arbitrary nanostructures. Therefore, there is a strong need to further develop this technique to meet industry processing requirements.

In order to realize an accurate and smooth scan patterning process, a gap between the focusing lens and sample is a necessary condition. In contrast, a contact mode may result in dragging issues due to lens-sample friction, which can lead to distortion of final patterns. In addition, unintentional scratches on delicate samples may also be generated. Most studies have focused on the microsphere lens patterning technique based on a near-field mode that is contact or within an incident wavelength distance. Recently, manipulation of a single microsphere lens by laser trapping and tip-based scanning techniques was demonstrated for complex nano-pattern processing [25,26]. They were both used in the near-field modes, either limited to

liquid environment (laser trapping) or involving a sophisticated and costly near-field tip control system. We wish to develop a far-field, low-cost, super-resolution microsphere scanning writing system for direct laser writing of arbitrary nano-patterns, which can be further extended to super-resolution imaging and sensing applications.

In this Letter, we report a major step forward in a laser direct patterning system that can perform large-area subwavelength surface processing with user-defined patterns. A new superlens design, namely a compound lens consisting of a plano-convex lens with a high-index microsphere lens (PCM), was proposed. The PCM superlens can be implemented as an optical probe to generate subwavelength focusing at micrometer distance. With the assist of a side-view monitoring system and high-resolution nano-stage, we can achieve precise control and monitoring of the working distance (WD) between the probe and sample during the scan patterning process. Meanwhile, the performance of the PCM lens at different WDs was theoretically and experimentally evaluated. The capability of arbitrary pattern fabrication was realized. It is an objective-free, low-cost, highly efficient, and flexible system with high completion for large-area subwavelength nano-patterning, which will satisfy the growing industrial demands in laser nano-patterning.

The experimental setup is illustrated in Figs. 1(a) and 1(c). The supporting frame was made of 3D printed structures and metal struts to install a lens and stages. A barium titanate glass (BTG) microsphere (BTGMS, Cospheric) with a diameter of 50  $\mu\text{m}$  was aligned and attached onto polydimethylsiloxane (PDMS; SYLGARD 184, DOW CORNING) or UV glue (NOA63, Noland Adhesive) pre-coated curved surface of a BK7 plano-convex lens (LA1700, Thorlabs). A second thin layer of PDMS or UV glue was then applied to form partial encapsulation of BTG microsphere by spin-coating at 2000 rpm for 1 min [Fig. 1(d)]. This results in the formation of a probe-like plano-convex-microsphere (PCM) lens, with a single microsphere slightly extruding [Fig. 1(e)]. Afterwards, the PCM lens was bonded onto a 3D printed lens holder to build a detachable PCM lens module [Fig. 1(b)]. A manual three-axis stage was used for coarsely adjusting the target sample. A long WD zoom lens was placed horizontally at the side for monitoring the gap between the microsphere tip and samples. The light sources were generated by a femtosecond laser consisting of a Ti:sapphire oscillator (Spectra Physics Tsunami) and a regenerative amplifier (Spectra Physics Spitfire) which provides an 800 nm wavelength, 100 fs pulse duration, and 5 KHz repetition rate. The beam diameter projected at the PCM lens incident plane was  $\sim 200 \mu\text{m}$ .

The scanning was performed using a high-resolution nano-stage (P-611.3 NanoCube, Physik Instrumente), with 1 nm resolution in the XYZ direction and a travel range of 100  $\mu\text{m}$ . In our experiments, the PCM lens was kept static, and the underlying nano-stage moved and scanned the samples across the PCM lens. The laser processing was automatically undertaken at the synchronization of the laser and nano-stage through an in-house developed GCS code. Samples, including silicon wafer, nickel, and Au thin film coated glass, were tested.

To understand focusing characteristics of the PCM lens, computational modelling was performed using in-house developed code based on physical optics. A plane wave (800 nm, x-polarized) propagates (along the z axis) through a 50  $\mu\text{m}$  BTG microsphere ( $n_p = 1.9$ ) partially encapsulated by PDMS

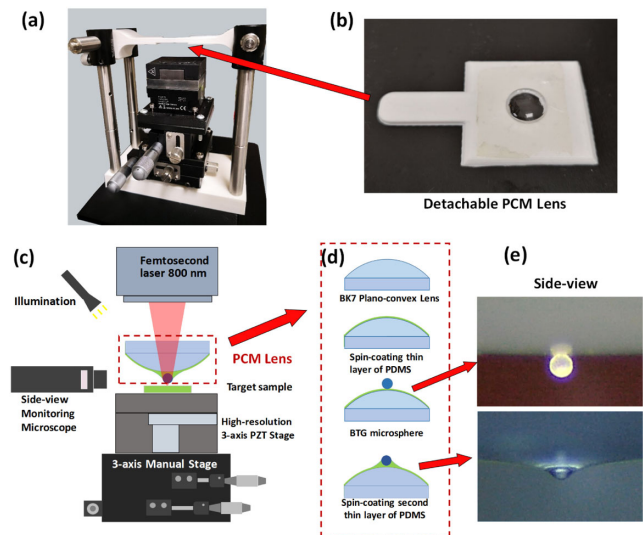


**Fig. 1.** PCM lens and system setup for laser nano-patterning. (a) Photograph of actual system setup. (b) Photograph of an actual detachable PCM lens module. (c) Schematic of the PCM nano-patterning system. (d) Fabrication of a PCM lens. (e) Side view of a PCM lens.

material ( $n_m = 1.4$ ) to imitate a PCM lens in the experiment. Figure 2(a) shows the calculated optical field distribution in the YZ plane. It reveals that the electric field intensity exhibits elongated shape and diverges with distance. The electric field intensity was greatly enhanced ( $\sim 2000$  times) at a 9.14  $\mu\text{m}$  distance away from a microsphere bottom boundary, and intensity drops quickly onwards. Figure 2(b) illustrates the field profiles along the y direction at different WDs. We observed multi-peak focusing phenomena before the light convergence and significant side-peak occurs around 7  $\mu\text{m}$  distance. The focal spot size with respect to the distances was revealed in Fig. 2(c). The calculated full-width at half-maximum (FWHM) starts from 200 nm at a boundary of microsphere, then gradually rises to 670 nm as the distance increases to 11  $\mu\text{m}$ ; afterwards, it reaches at micro-scale due to light divergence. The super-resolution ( $\lambda/2 < 400 \text{ nm}$ ) is found for distances within 6  $\mu\text{m}$  measured from the bottom of the PCM lens.

To verify the theoretical analysis, experiments were carried out by a femtosecond 800 nm wavelength laser with fluence of  $9.5 \pm 0.2 \text{ mJ}/\text{cm}^2$ . A blank silicon wafer was initially elevated to moderately contact the PCM lens by a nano-stage, and then lowered with 1  $\mu\text{m}$  step until 16  $\mu\text{m}$  apart. A laser was triggered at each WD, and patterned features are shown in Fig. 2(d). Figures 2(e)–2(p) are the enlarged SEM images at a WD from 2 to 13  $\mu\text{m}$ . There was no feature observed at distances of 1  $\mu\text{m}$  and 14–16  $\mu\text{m}$  because of the low field enhancement or large focal spot in these regions resulting in the power density less than the silicon damage threshold, as the simulation result shown in Fig. 2(c). At WD = 2  $\mu\text{m}$ , the theoretical super-resolution focus spot size is 320 nm [ $\lambda/2.50$ , Fig. 2(c)]. In experiments, however, we achieved a smaller feature size down to 230 nm [ $\lambda/3.48$ , Fig. 2(e)]; this is due to the nonlinear multiphoton absorption effect when the femtosecond laser pulse interacts with materials [27]. The feature size increased gradually afterwards to around 1  $\mu\text{m}$  at WD = 4  $\mu\text{m}$ . It is noted that at distances of 6, 7, and 8  $\mu\text{m}$ , features exhibited not only single hole, but also outer ring

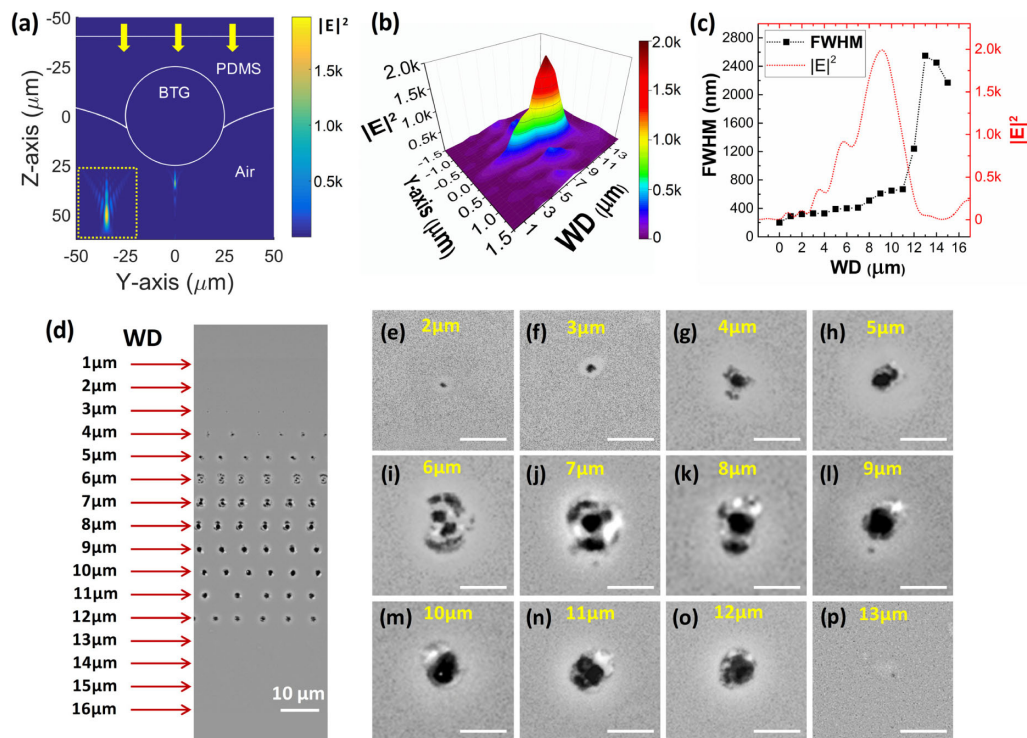


**Fig. 2.** Modelling of PCM lens focusing properties and experimental results of a femtosecond laser machined feature size against the WD. (a) Electric field intensity  $|E|^2$  distribution of a PCM lens across the YZ incident plane; the inset shows the enlarged view of the focusing area. (b) Field distribution along the y axis and (c) FWHM and  $|E|^2$  enhancement at different WDs. (d) Femtosecond laser patterned feature at a WD from 1 to 16  $\mu\text{m}$  and (e)–(p) enlarged SEM images at 2–13  $\mu\text{m}$  distances; the scale bars in (e)–(p) are 2  $\mu\text{m}$ .

patterns simultaneously [Figs. 2(d), and 2(i)–2(k)]. This may be determined by the multiple peaks effect, which is consistent with previously discussed theoretical simulation results, shown in Fig. 2(b). Therefore, high-quality laser marking should avoid such circumstances. Meanwhile, the sharpest and roundest hole pattern was found at the distance of 9  $\mu\text{m}$  [see Fig. 2(i)], which can be seen as the processing focus point. Furthermore, Fig. 2(p) shows a very shallow and unclear dot generated at 13  $\mu\text{m}$  away from the PCM lens. In general, the experimental results agreed well with the simulation model, and the smallest feature size is mainly determined by the PCM lens WD and laser power density.

In the scanning patterning mode, a laser was synchronized with the maneuver of the piezo nano-stage by an in-house developed controlling code, which controlled the laser beam on and off while the sample moved to realize accurate positioning machining. A blank silicon wafer was scanned over an area in a non-contact mode with a 2  $\mu\text{m}$  distance under the PCM lens, thus avoiding the undesired scratches and distorted pattern from friction between the lens and samples. Here we presented two scanning modes: point-by-point and continuous mode. In the point-by-point mode, the laser emits a pulse when the nano-stage completes a step. Therefore, the pattern outline is formed by dots with a certain interval, as shown in Figs. 3(a) and 3(b). Possibly due to system vibration and fluctuations (e.g., laser fluence and scanning system) during experiments, the obtained dots have a size variation ranging from 230 to 350 nm. On the other hand, Figs. 3(c) and 3(d) show that the continuously processed line can be generated by keeping the

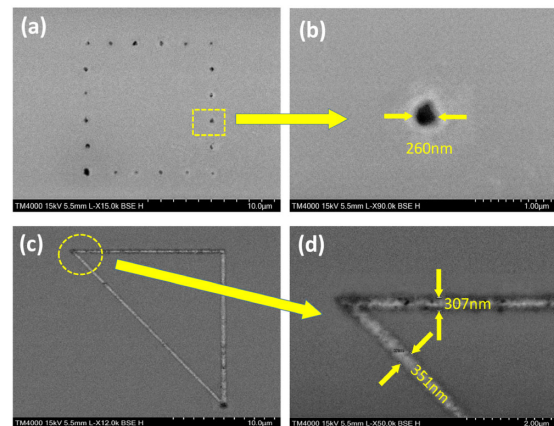


**Fig. 3.** Scanning patterning by (a) and (b) point-by-point and (c) and (d) continuous mode.

laser constantly on during sample moving. In this case, the line size is about 300–350 nm.

Furthermore, it is important to know that the proposed system is not limited to fabricating simple line and dot patterns, but also flexible enough to write user-defined complex patterns. Arbitrary pictures can be directly converted into nano-stage recognizable GCS code by a self-developed Java program. Therefore, the sample's moving path followed the exact shape from original pictures. The capability of writing complex arbitrary patterns was evaluated, shown in Fig. 4. Meanwhile, we have extended this method to other materials, such as nickel

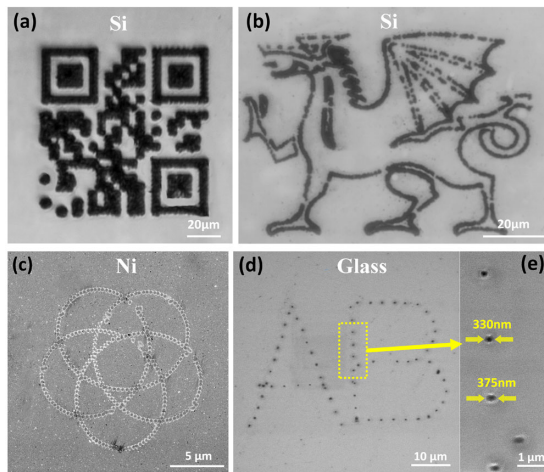


**Fig. 4.** Arbitrary patterns on different sample surfaces. On a silicon wafer: (a) Bangor University website QR code, (b) Welsh dragon. (c) Guilloche pattern on nickel substrate, (d) letters on a glass substrate, (e) enlarged image of highlighted area in (d).

[Fig. 4(c)] and glass substrate [Figs. 4(d) and 4(e)]. The average processing resolution on glass substrate was measured as 354 nm. Compared to the CPLA technique for a simple structure in a limited area, our system provides a more flexible way for large-area patterning. Moreover, this technique can be further developed by using a shorter wavelength laser such as a UV laser (355 nm) to improve the patterning resolution down to about 100 nm. The PCM lens can naturally be extended to other super-resolution applications, including nano-imaging, sensing, trapping, and manipulation of nano-objects and samples [28,29].

In summary, we have proposed and demonstrated a new PCM superlens that can be operated in a far-field scanning manner to effectively process complex arbitrary patterns in a subwavelength scale. The effect of non-contact patterning was evaluated theoretically and experimentally at different WDs. The individual subwavelength features of a size as small as 230 ( $\lambda/3.48$ ) – 350 nm ( $\lambda/2.29$ ) can be directly fabricated. The large-area complex structures with arbitrary shapes can be easily generated. Meanwhile, the reliability and repeatability were significantly improved compared to other microsphere-based laser fabrication techniques. The development is low-cost and compatible with any existing laser marking system to enhance the patterning resolution.

**Funding.** Center for Photonics Expertise; European Regional Development Fund (81400); Knowledge Economy Skills Scholarship (BUK289).

## REFERENCES

1. E. Abbe, Arch. für mikroskopische Anat. **9**, 413 (1873).
2. T. C. Chong, M. H. Hong, and L. P. Shi, *Laser Photonics Rev.* **4**, 123 (2010).
3. E. Betzig, J. K. Trautman, R. Wolfe, E. M. Gyorgy, P. L. Finn, M. H. Kryder, and C. H. Chang, *Appl. Phys. Lett.* **61**, 142 (1992).
4. Y. F. Lu, Z. H. Mai, Y. W. Zheng, and W. D. Song, *Appl. Phys. Lett.* **76**, 1200 (2000).
5. Z. W. Liu, Q. H. Wei, and X. Zhang, *Nano Lett.* **5**, 957 (2005).
6. L. P. Shi and T. C. Chong, *J. Nanosci. Nanotechnol.* **7**, 65 (2007).
7. M. Bieda, M. Siebold, and A. F. Lasagni, *Appl. Surf. Sci.* **387**, 175 (2016).
8. R. Ahmed, A. K. Yetisen, A. El Khoury, and H. Butt, *Nanoscale* **9**, 266 (2017).
9. S. Kawata, H. B. Sun, T. Tanaka, and K. Takada, *Nature* **412**, 697 (2001).
10. M. Aeschlimann, M. Bauer, D. Bayer, T. Brixner, F. J. G. De Abajo, W. Pfeiffer, and F. Steeb, *Nature* **446**, 301 (2007).
11. Z. Chen, A. Taflove, and V. Backman, *Opt. Express* **12**, 1214 (2004).
12. S. Lecler, Y. Takakura, and P. Meyrueis, *Opt. Lett.* **30**, 2641 (2005).
13. Y. F. Lu, L. Zhang, W. D. Song, Y. W. Zheng, and B. S. Luk'Yanchuk, *J. Exp. Theor. Phys. Lett.* **72**, 457 (2000).
14. E. McLeod and C. B. Arnold, *Nat. Nanotechnol.* **3**, 413 (2008).
15. E. McLeod and C. B. Arnold, *Opt. Express* **17**, 3640 (2009).
16. S. M. Huang, M. H. Hong, B. Luk'yanchuk, and T. C. Chong, *Appl. Phys. A* **77**, 293 (2003).
17. Z. B. Wang, M. H. Hong, B. S. Luk'yanchuk, Y. Lin, Q. F. Wang, and T. C. Chong, *J. Appl. Phys.* **96**, 6845 (2004).
18. Z. B. Wang, M. H. Hong, B. S. Luk'yanchuk, S. M. Huang, Q. F. Wang, L. P. Shi, and T. C. Chong, *Appl. Phys. A* **79**, 1603 (2004).
19. W. Guo, Z. B. Wang, L. Li, D. J. Whitehead, B. S. Luk'yanchuk, and Z. Liu, *Appl. Phys. Lett.* **90**, 243101 (2007).
20. N. Denkov, O. Velez, P. Kralchevski, I. Ivanov, H. Yoshimura, and K. Nagayama, *Langmuir* **8**, 3183 (1992).
21. M. Mosbacher, H. J. Münzer, J. Zimmermann, J. Solis, J. Boneberg, and P. Leiderer, *Appl. Phys. A* **72**, 41 (2001).
22. C. O'Connell, R. J. Sherlock, and T. J. Glynn, *Opt. Eng.* **49**, 014201 (2010).
23. A. Khan, Z. Wang, M. A. Sheikh, D. J. Whitehead, and L. Li, *J. Phys. D* **43**, 305302 (2010).
24. A. Khan, Z. Wang, M. A. Sheikh, D. J. Whitehead, and L. Li, *Appl. Surf. Sci.* **258**, 774 (2011).
25. A. Shakhov, A. Astafiev, A. Gulina, and V. Nadtochenko, *ACS Appl. Mater. Interface* **7**, 27467 (2015).
26. Y. Wen, H. Yu, W. Zhao, F. Wang, X. Wang, L. Liu, and W. J. Li, *IEEE Trans. Nanotechnol.* **18**, 226 (2019).
27. S. S. Harilal, J. R. Freeman, P. K. Diwakar, and A. Hassanein, *Laser-Induced Breakdown Spectroscopy* (Springer, 2014), p. 143.
28. Z. Wang, W. Guo, L. Li, B. Luk'yanchuk, A. Khan, Z. Liu, Z. Chen, and M. Hong, *Nat. Commun.* **2**, 218 (2011).
29. B. S. Luk'yanchuk, R. Paniagua-Dominguez, I. Minin, O. Minin, and Z. B. Wang, *Opt. Mater. Express* **7**, 1820 (2017).